JOURNAL OF THERMOPHYSICS AND HEAT TRANSFER
Vol. 10, No. 2, April–June 1996

Performance Characteristics of a Stainless Steel/Ammonia Loop Heat Pipe

Paul J. Wirsch* and Scott K. Thomas†
Wright State University, Dayton, Ohio 45435

The purpose of this study is to experimentally determine the operating characteristics of a stainless steel/ammonia loop heat pipe for vapor line temperatures of 40 and 50°C. Previous experimental research efforts have not attempted to control the vapor temperature of the loop heat pipe. Instead, the coolant and/or condenser temperatures have been controlled. For comparison with future analytical and numerical models of the loop heat pipe, the vapor temperature, which is normally close to saturation conditions, may be a better indicator of the operating condition than the coolant or condenser temperatures. The thermal resistance, temperature distribution, evaporative heat transfer coefficient for an inverted meniscus evaporator, and the capillary limit were determined as functions of the vapor temperature for a horizontal orientation. A two-dimensional numerical model of the evaporator section was developed and verified using the experimental results. The evaporative heat transfer coefficient for an inverted meniscus evaporator determined from the experimental results was used in the numerical model as a convective boundary condition. The comparison between the experimental and numerical results shows good agreement, indicating that the evaporator section has been accurately modeled.

Nomenclature

D = i.d. of the evaporator, m
d = diameter of the liquid and vapor lines, m
H = height, m
h = convective heat transfer coefficient, W/m^2 K
k = thermal conductivity, W/m K
L = length, m
n = normal direction
$\dot{Q}$ = heat rate, W
$\dot{q}$ = heat flux, W/m^2
R = thermal resistance, K/W
r = radial coordinate, m
T = temperature, K
t = thickness, m
W = width, m
x, y = Cartesian coordinates, m
ϕ = temperature, K

Subscripts

a = aluminum
ab = ambient
c = condenser
cf = cooling fluid
dry = dryout
e = evaporator section
eff = effective
g = thermal grease
h = heater
i = inner
o = outer
rad = radiator
ss = stainless steel
v = vapor
1 = inner wall of the evaporator
2 = outer wall of the evaporator
3 = inner wall of the aluminum saddle

Received July 10, 1995; revision received Sept. 12, 1995; accepted for publication Sept. 15, 1995.

*Graduate Research Assistant, Department of Mechanical and Materials Engineering. Member AIAA.
†Assistant Professor, Department of Mechanical and Materials Engineering. Member AIAA.

Introduction

THREE capillary-driven thermal management systems have been developed with space-based applications: heat pipes, capillary pumped loops (CPLs), and loop heat pipes (LHPs). Heat pipes were invented by Gaugler[1] and then reinvented in the 1960s at the Los Alamos National Laboratory. Heat pipes are relatively simple devices that have been used in many space-based and terrestrial applications. The CPL was developed by Stenger[2] and is significantly more complicated to build and operate than a heat pipe. For this reason CPLs are still in the developmental stage and have not been applied to many situations. The LHP was developed by Maidanik and co-workers at the Laboratory of Heat Transfer Devices, Institute of Thermal Physics, Ural Branch of the USSR Academy of Sciences in the early 1980s.[3,4] Advantages of the LHP over the CPL include a self-priming ability, and the fact that the LHP does not require an external pump or heater on the reservoir to prime the evaporator. The LHP does not have the liquid entrainment losses from the liquid–vapor interface or the liquid flow losses in the wick structure of a conventional heat pipe. The space-based applications of the LHP include electronics cooling, reactor power conversion system waste heat rejection, and cryocoolers. Terrestrial applications are downward pumping solar collectors, cryorefrigerators, and electronics cooling.

The operation of a typical LHP begins with the application of heat to the evaporative zone, which evaporates the working fluid. The vapor is then collected by grooves in the porous insert (inverted meniscus evaporator). As the vapor travels the length of the evaporator through the vapor grooves it becomes slightly superheated because the inner wall temperature of the evaporator is higher than the saturation temperature. The vapor is forced into the vapor line by the pressure difference between the evaporator and condenser. The working fluid then enters the condenser section and condenses on the tapered walls. The liquid flows down the length of the tapered annulus by gravity and capillary pressure where it is subcooled. The subcooled liquid returns to the reservoir (or compensation cavity) by the capillary pumping pressure of the wick structure. The subcooled liquid is distributed to the

evaporator from the reservoir through a small annulus as needed. If the reservoir was drained completely, there would still be enough liquid to saturate the wick, making the LHP self-priming.

Maidanik et al.[5] performed tests on a prototype LHP in a horizontal position while increasing the input power to the evaporator from $\dot{Q}_e$ = 5 to 300 W (up to $\dot{q}_e$ = 7.1 W/cm^2) to determine the operating characteristics. The condenser cooling fluid temperatures were varied from T_{cf} = 30, 0, and −15°C. The results of the tests were deemed acceptable and used to design another LHP. This second model developed was named the Alyona and was built to be tested in a microgravity environment. The first tests conducted were performed in a vacuum chamber with the ambient temperature ranging from T_a = 18 to 22°C. Tests showed that ammonia could not be used as a working fluid in space because of its relatively high freezing temperature. Therefore, propene was used. The maximum power achieved during the ground tests was $\dot{Q}_e$ = 100 W, while in space the LHP transported a maximum heat rate of $\dot{Q}_e$ = 1398 W ($\dot{q}_e$ = 6.4 W/cm^2). The authors concluded that the flight and ground tests showed that the LHP was reliable for startups in which the input power was suddenly applied to the evaporator.

Dickey and Peterson[6] tested an LHP with the expectations of comparing the result to a conventional heat pipe. The condenser temperature was held constant at T_c = 30 and 0°C, while the input power was increased in increments of 10 W for T_c = 0°C and 20 W for T_c = 30°C. The difference in height between the evaporator and condenser (evaporator above the condenser) was varied from H = 0 to 61 cm. A steady-state numerical model was derived based on energy balances over the evaporator and condenser sections. The model was able to predict the average vapor temperature, average liquid temperature, and mass flow rate. While the experimental results were in good agreement with the numerical results, the researchers did not exceed an input power of $\dot{Q}_e$ = 170 W ($\dot{q}_e$ = 3.7 W/cm^2).

Meyer et al.[7] performed a series of five tests on an LHP. The first test was to determine the maximum power input. This test was performed with the evaporator 2 m above the condenser. The LHP was capable of transporting $\dot{Q}_e$ = 1129 W ($\dot{q}_e$ = 8.0 W/cm^2, estimated) before exceeding the maximum evaporator temperature of T_e = 90°C. During this test, the cooling liquid for the condenser was held between T_{cf} = 10–30°C to maintain acceptable temperatures in the evaporator. The second set of tests determined if the orientation of the LHP (vapor line above liquid line or vice versa) from 5 to 25 mm had a significant effect. The results showed a temperature difference between the evaporator and condenser of only ΔT_{ec} = 1°C, with the height between 5–25 mm. The third area of testing included startup procedures. These tests ranged from the LHP being horizontal, vertical with the evaporator on the top, and vertical with the evaporator on the bottom. The researchers had no problems starting the LHP under the first and third test conditions, but the condition in the second set of tests required a large step power input after the initial startup in this position. The fourth and fifth tests dealt with repriming the evaporator after dryout and load variation responses, respectively. The LHP reprimed successfully after 50 s and demonstrated an ability to remain stable during load variations.

Ernst et al.[4] reported repeatable data from an LHP, which was originally built as a backup for testing on the Soviet spacecraft Granat that transported $\dot{Q}_e$ = 120 W with H = 1.5 m and $\dot{Q}_e$ = 225 W with H = 2.75 m. A separate LHP was installed in a vacuum chamber with a radiator configured to the condenser while holding the walls of the vacuum chamber at T_a = 193 K. The experiments showed a change in temperature from the evaporator to condenser of ΔT_{ec} = 5.9 K at $\dot{Q}_e$ = 25 W with a radiator temperature of T_r = 266.7 K, ΔT_{ec} = 10.8 K at $\dot{Q}_e$ = 50 W with T_r = 296.6 K, and ΔT_{ec} = 21.9 K at $\dot{Q}_e$ = 120 W with T_r = 335.5 K. The LHP was also installed in the spacecraft Granat to determine the effects of a microgravity environment on a device of this type. Also discussed were the applications of the LHP, such as electronics cooling, power conversion system waste heat rejection, cryocoolers, and downward-pumping solar collectors.

The purpose of the present study was to determine the heat transfer characteristics of a stainless steel/ammonia loop heat pipe for vapor line temperatures of T_v = 40 and 50°C and to develop a numerical model of the evaporator section. Experimentally, previous researchers have held the condenser and/or coolant temperature constant, which may not be appropriate due to inaccuracies in reading this type of temperature. Measuring the vapor temperature in an adiabatic region is much more reliable. For comparison with future analytical and numerical models of the LHP, the vapor temperature may be more appropriate in setting the operating condition of the LHP because it is usually very close to saturation conditions. Also, the degree of superheating is extremely small due to the closed-loop nature of the LHP. This experimental methodology may provide a more realistic comparison for the maximum heat transport limit for different loop heat pipes since matching saturated conditions can be more closely achieved than matching conditions at the condenser section. The thermal resistance, temperature distribution, evaporative heat transfer coefficient for an inverted meniscus, and capillary limit of the LHP were determined as functions of the vapor temperature for a horizontal orientation. A two-dimensional finite element model was developed and verified by the experimental results. The evaporative heat transfer coefficient for an inverted meniscus determined in the experimental section was used as the convective boundary condition in the numerical model.

Experimental Setup and Procedure

The stainless steel/ammonia LHP consisted of an evaporator, condenser, reservoir, and interconnecting piping. The evaporator was equipped with a cylindrical sintered nickel powder wick structure, which had a porosity of 70%. The evaporator and condenser had flat aluminum saddles that were push-fitted onto the sections for heat load addition and rejection. The evaporator section had two specially mounted strip heaters to supply energy into the system. A 1.27-cm-thick Teflon® housing was used to hold the heaters in place and for insulation to minimize heat losses to the environment. The copper cooling reservoirs mounted on the condenser section were constructed out of 1.58-cm-thick copper plates that were cut to the size of the condenser saddle. These plates were milled to form an interior chamber 2.54 cm wide × 11.43 cm long × 1.27 cm deep. The corners of the chamber were rounded so that air pockets would not form when coolant flowed through the chamber. Holes were provided on the ends for fluid flow inlets and outlets. Neoprene gaskets were used to seal the copper cooling reservoirs to the condenser saddle. The interconnecting lines were constructed out of stainless steel with a smooth bore in both the liquid and vapor lines. The liquid line had an o.d. of d_o = 3 mm and an i.d. of d_i = 2 mm. For the vapor line, d_o = 4 mm and d_i = 3 mm.

Insulation was wrapped around the evaporator, condenser, reservoir, and liquid and vapor lines at a thickness of 2.54 cm to minimize the influence of the environment. The test stand consisted of a mounting table for the LHP that was 3.96 m in length and housed the 3.81-m-long LHP, which was fully extended. The stand was built to study the effects of transient and steady-state operation of the LHP at different inclination angles.

The heat source consisted of two 200-W strip heaters, a variable a.c. transformer, and two multimeters. The heaters were 2.54 × 10.16 cm and were mounted on each side of the

evaporator section. The power supplied to the heaters was controlled by a 110-V variable a.c. transformer. One multimeter monitored the voltage input to the heaters and a magnetic current probe was used to monitor the amperage. The uncertainty for the power input was ±2% of the reading.

The heat sink consisted of two recirculating chilling units, which circulated coolant through the copper cooling reservoirs that were mounted on the top and bottom of the condenser section. One chiller was connected to the top plate and the other was connected to the bottom in a countercurrent configuration. The coolant fluid that was used had a 1:1 mixture of water and ethylene glycol. A flow meter with a stainless steel float was used during calibration of the calorimeter, where it was found that the difference between the power input into the evaporator and the power output from the condenser was less than 10%. Therefore, the power input is given in the discussion of the results.

The data acquisition system had a built-in digital input board that read the potential from the thermocouples. This system also had a direct interfacing card to a personal computer. The accuracy of the thermocouples was determined by placing them into the chiller bath over the expected temperature range. This data was then used to find the mean and standard deviation of the readings of each thermocouple. The uncertainty of the thermocouple readings was found to be ±0.41 K. The thermocouples were placed at critical points along the LHP. Four thermocouples were cemented into the holes in the aluminum saddle along the evaporator. These holes extended to the o.d. of the stainless steel evaporator section. One thermocouple was placed on the reservoir. Three thermocouples were placed on the liquid and vapor lines, the locations of which were 30 cm from the evaporator and condenser and at the middle of each line. Four thermocouples were placed on the condenser in the same manner as the evaporator. The coolant lines had thermocouples at the inlets and outlets of the calorimeter so that the heat output could be calculated. An average temperature was reported for the evaporator and condenser sections by calculating the mean temperature of the four thermocouples placed in each section. The largest standard deviation for the average evaporator temperature was 2.81°C.

The operating procedure for the heat pipe was conducted in steps and allowed at each step to achieve a steady-state condition. The first step was the setting of the chillers to cool the condenser. The flow rate and temperatures were set depending on the operating temperature that was desired. Once the condenser section was at a steady-state temperature, the power to the evaporator was turned on. When the power to the evaporator reached $\dot{Q}_e$ = 140 W, recording of data was started. The power was increased by increments of approximately 10–15 W. During a test, the vapor line was monitored to ensure that the LHP was operating at a constant vapor line temperature. If needed, modifications were made in the chiller temperatures and flow rates to maintain the specified vapor temperature. After each power increase, the system was allowed to achieve and be maintained at the steady state for at least 40 min. Data was recorded every 2 min from the time of the power increase until the end of the steady-state time period. The chiller temperatures and flow rates were changed accordingly to maintain the vapor line temperature as the power was increased. This was done until dryout was reached or the maximum power capabilities of the evaporator heaters or condenser chillers were reached. Dryout describes the condition when the wick structure of the evaporator is not provided with a sufficient amount of working fluid. Therefore, the evaporator temperature increases rapidly. This is the result of an excessive heat flux applied to the evaporator. Once the maximum power setting had been reached or the evaporator dried out, power to the evaporator heaters was shut off. A complete discussion of the experimental setup is given by Wirsch.[8]

Numerical Modeling of the Evaporator Section

The evaporator section of the LHP is modeled numerically and the results are validated using the experimental data for vapor temperatures of T_v = 40 and 50°C. The evaporator section consists of a cylindrical stainless steel evaporator with an inverted meniscus porous insert, an aluminum saddle of rectangular cross section into which the evaporator is push-fitted, and a thin layer of thermal grease between the stainless steel and the aluminum to improve thermal contact. The operation of the evaporator begins with the application of heat to the aluminum saddle (Figs. 1a and 1b) by two strip heaters. The applied heat flux is then conducted through the aluminum saddle, thermal grease, and the stainless steel wall of the evaporator. On the inner wall of the evaporator the ammonia working fluid is evaporated and collected by grooves in the porous insert (inverted meniscus evaporator). The vapor is then forced into the vapor line by the pressure difference between the evaporator and condenser. While the vapor is being forced out of the evaporator section, subcooled liquid is supplied to the evaporator by the capillary wick structure.

A finite element analysis technique was employed to model the conduction heat transfer in the evaporator. The model (Fig. 1) considered heat input from the heaters to the aluminum saddle. From the interface of the heaters and the aluminum saddle, heat energy was conducted through the aluminum saddle to the evaporator via the layer of thermal grease. The inside radius of the evaporator wall had an evaporative convection boundary condition. At the interfaces between the thermal grease and the aluminum saddle, and the stainless steel and the thermal grease, the temperature was continuous and the energy balances were preserved. The remaining boundary conditions were considered to be adiabatic due to insulation and the symmetry of the model. The assumptions used in the development of the model are as follows:

1) A steady-state two-dimensional analysis is used in which end effects are considered to be negligible.

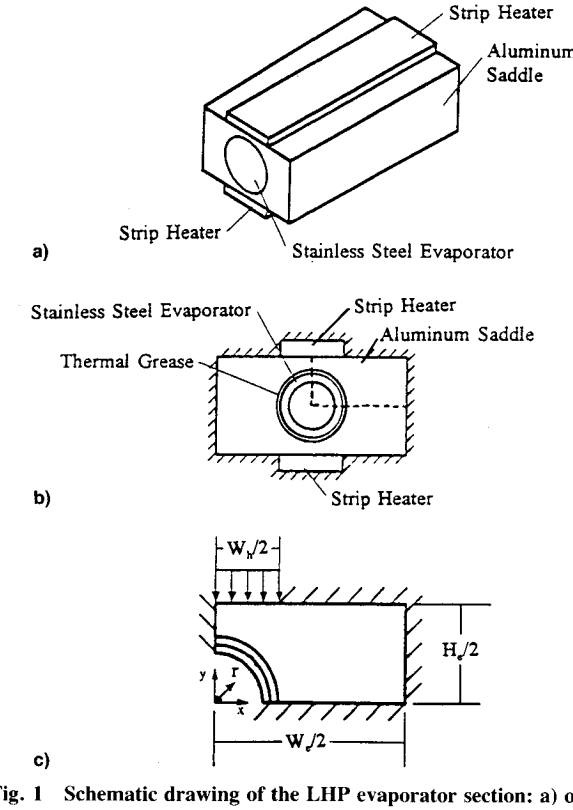

Fig. 1 Schematic drawing of the LHP evaporator section: a) overall evaporator section, b) cross section of the evaporator, and c) solution domain.

2) The heat flux from the heaters is constant along the width of the heaters.

3) All remaining external surfaces of the aluminum saddle are adiabatic due to insulation.

4) Quarter symmetry is used for modeling the evaporator section as seen in Figs. 1b and 1c. This does not affect the accuracy of the results, but is less computationally intensive.

5) Constant properties within the three regions (aluminum saddle, thermal grease, and stainless steel evaporator) were assumed.

The steady-state two-dimensional heat conduction equation is given by

$$\nabla^2 T = 0 \tag{1}$$

The boundary conditions that were applied to the cross section (Fig. 1c) consist of a constant heat flux applied by the heater to the aluminum saddle at $y = 0.5H_c$ and $0 \le x \le 0.5W_h$. This condition was described by the Fourier law of heat conduction:

$$q_c'' = -k_a \frac{\partial T}{\partial y} \tag{2}$$

where q_c'' is the heat flux supplied from the strip heaters and k_a is the thermal conductivity of the aluminum saddle. Along the outside edges of the evaporator, insulation was placed from $y = 0.5H_c$ and $0.5W_h \le x \le 0.5W_c$, and $x = 0.5W_c$ and $0 \le y \le 0.5H_c$. At these locations the boundaries were considered to be adiabatic. The planes of symmetry at $y = 0$ and $r_1 \le x \le 0.5W_c$ and at $x = 0$ and $r_1 \le y \le 0.5H_c$ were also considered to be adiabatic. At these locations the boundary condition was described by

$$k_i \frac{\partial T}{\partial n} = 0 \tag{3}$$

where n is the direction normal to the surface in question and k_i describes the thermal conductivity of the three regions:

$$k_i = \begin{cases} k_a & \text{aluminum} \\ k_{ss} & \text{stainless steel} \\ k_g & \text{thermal grease} \end{cases}$$

At the inner radius of the stainless steel evaporator, a convective boundary condition is applied to simulate evaporation from the inverted meniscus:

$$-k_{ss} \frac{\partial T}{\partial r} = h(T - T_v) \quad \text{at} \quad r = r_1 \tag{4}$$

where T_v is the mean temperature of the vapor.

At the two interfaces, aluminum/thermal grease and thermal grease/stainless steel, the continuity of temperature and the energy balances are given as

$$T_a = T_g \quad \text{at} \quad r = r_3 \tag{5}$$

$$T_g = T_{ss} \quad \text{at} \quad r = r_2 \tag{6}$$

$$k_a \frac{\partial T}{\partial n} = k_g \frac{\partial T}{\partial n} \quad \text{at} \quad r = r_3 \tag{7}$$

$$k_g \frac{\partial T}{\partial n} = k_{ss} \frac{\partial T}{\partial n} \quad \text{at} \quad r = r_2 \tag{8}$$

Numerical Solution Procedure

The heat conduction equation can be put into finite element form by applying the steady-state, two-dimensional assumptions:

$$\nabla^2 \phi = 0 \tag{9}$$

Table 1 Representation of boundary conditions in finite element form

Boundary condition	Description	k_i	M	N
2	Constant heat flux	k_a	0	$-q_c''$
3	Adiabatic	k_a, k_g, k_{ss}	0	0
4	Convection	k_{ss}	h	hT_v

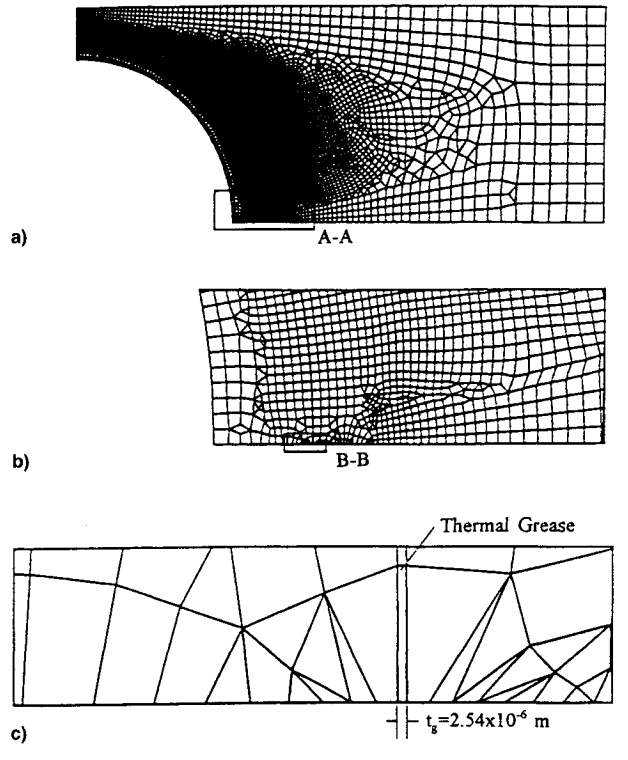

Fig. 2 Distribution of the grid structure for the evaporator section: a) overall view; b) section A-A, magnification of the grid structure surrounding the thermal grease; and c) section B-B, increased magnification of the grid structure surrounding the thermal grease.

where $\phi = T$. The adiabatic, convective, and constant heat flux boundary conditions can be represented in finite element form by the derivative boundary condition

$$k_i \frac{\partial \phi}{\partial n} = -M\phi + N \tag{10}$$

For each boundary condition there are different values for k_i, M, and N. Table 1 presents the boundary condition and the appropriate substitutions for k_i, M, and N. However, the continuity of temperature and energy balances [Eqs. (5–8)] are maintained implicitly by the finite element model.

Specification of the grid structure was dictated by the thermal grease. The thickness of the thermal grease $t_g = r_3 - r_2$ was very small in comparison to the thickness of the evaporator wall and the aluminum saddle. As such, a very fine mesh was employed in that region. To eliminate the need for excessive computer memory and CPU time, the grid structure was "grown" outward from the thermal grease. The grid structure of the thermal grease was one element thick in the radial direction. From this point, the grid structure progressed through the evaporator wall and the aluminum saddle with the element sizes becoming larger with distance from the thermal grease (Fig. 2). This type of grid structure was acceptable because the area where the temperature gradients were steepest was in the vicinity of the thermal grease.

After the model had been written and achieved accurate results (discussed in the following section) a grid independence test was performed. The grid independence test is the method by which the grid structure can be verified to be sufficiently fine. A second model was written with approximately 15% fewer elements (5718 vs 6740 elements). Selected results of both models showing temperature and location were plotted and it was shown that the maximum temperature difference between the two models was 0.069°C.

Results and Discussion

The purpose of the experiments was to determine the operating characteristics and the maximum heat transport rate of the stainless steel/ammonia LHP. Typical transient responses of the LHP at high heat inputs are shown in Figs. 3 (T_v = 40°C) and 4 (T_v = 50°C). As can be seen in Fig. 3a, the initial response time of the LHP is on the order of approximately 20 min, with fully steady-state conditions reached in 1 h. In all of the tested cases, the vapor line temperature and that of the reservoir were identical to within the accuracy of the instrumentation. Therefore, the reservoir and the vapor line were consistently at saturation conditions and the reservoir was at least partially filled with liquid at all times. This resulted in repeatable responses to step heat inputs to the LHP. At least two tests were performed for each setting to ensure repeatability. Since the liquid line passed through the reservoir; the working fluid in the liquid line (subcooled) was heated by that in the reservoir (saturated). Dryout was not reached for T_v = 40°C because the chillers were unable to dissipate the heat load after the input power exceeded $\dot{Q}_e$ = 260 W. As shown in Fig. 3, the average evaporator temperature increased with increasing power, while the condenser temperature remained nearly constant.

Figure 4 shows typical transient responses of the LHP for a vapor line temperature of T_v = 50°C. Oscillations in the condenser and liquid line temperatures were the result of the deadband range of one of the chillers (±1°C). These temperature fluctuations were not transmitted to the reservoir, evaporator, or vapor line. Unlike a conventional heat pipe, the evaporator and condenser temperatures of the LHP were significantly different than the vapor temperature. Therefore, the benefit of separating the liquid and vapor flows is accompanied by a large superheat penalty between the evaporator and condenser. Figure 4c demonstrates the occurrence of dryout in the evaporator section at $\dot{Q}_{e,\mathrm{dry}}$ = 337 W ($\dot{q}_{e,\mathrm{dry}}$ = 13.1 W/cm^2). A drastic increase in temperature in the evaporator can be seen where the capillary pumping pressure was insufficient to maintain the flow of liquid through the wick structure. This temperature increase in the evaporator also caused the vapor and reservoir temperatures to increase due to the sudden influx of higher-temperature superheated vapor from the evaporator. The condenser temperature dropped because the flow rate of vapor from the evaporator decreased as dryout progressed.

The steady-state operating characteristics of the LHP are shown in Fig. 5 as functions of the input power to the evaporator section. Figure 5a shows the steady-state temperature difference between the evaporator and condenser sections.

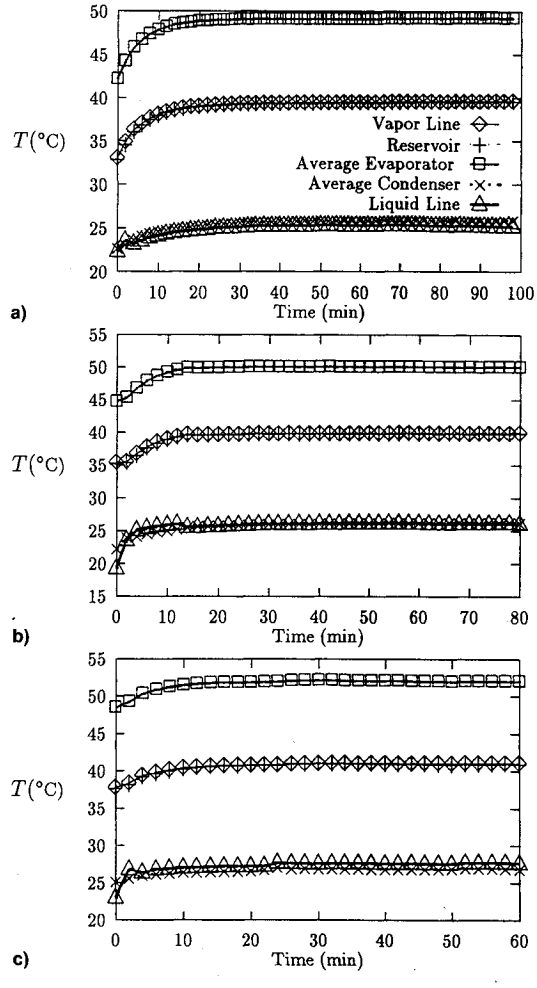

Fig. 3 Experimental transient temperature profiles for T_v = 40°C and power inputs of $\dot{Q}_e$ = a) 220–230, b) 230–240, and c) 250–260 W.

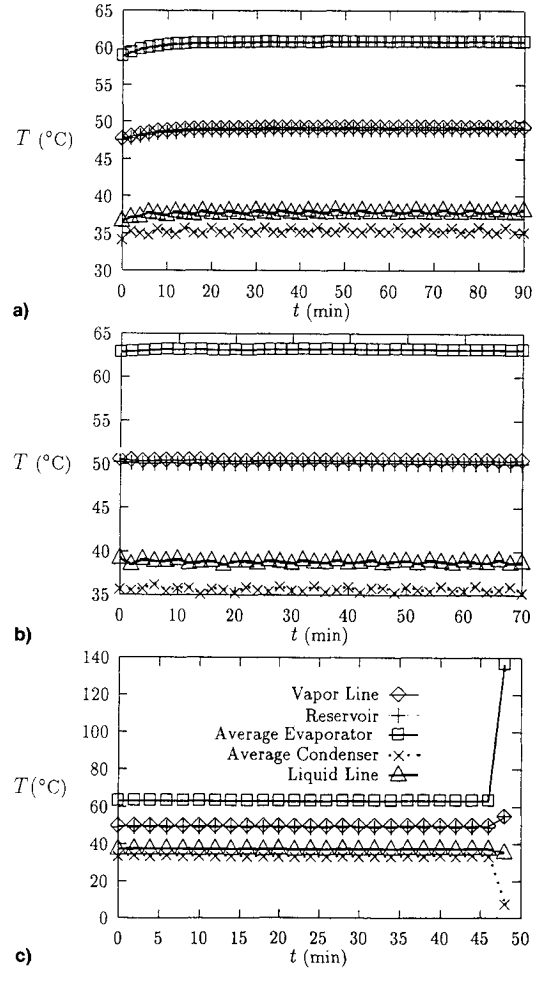

Fig. 4 Experimental transient temperature profiles for T_v = 50°C and power inputs of $\dot{Q}_e$ = a) 274–288, b) 303–316, and c) 326–337 W (dryout).

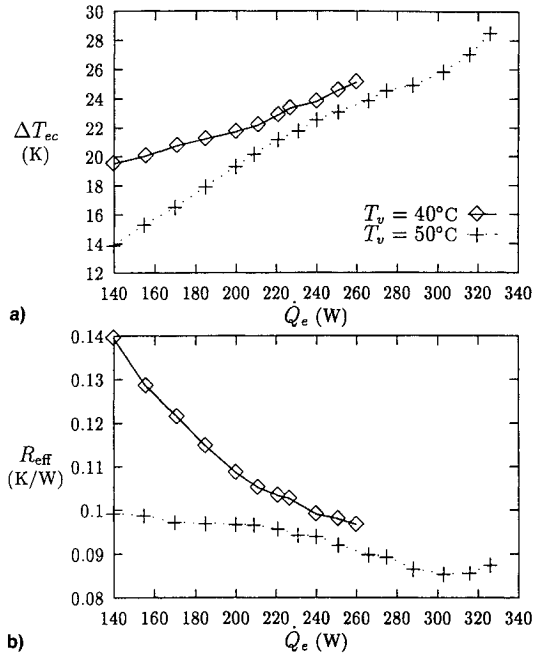

Fig. 5 Experimental steady-state operating characteristics of the LHP as functions of input power: a) evaporator-to-condenser temperature difference and b) effective thermal resistance.

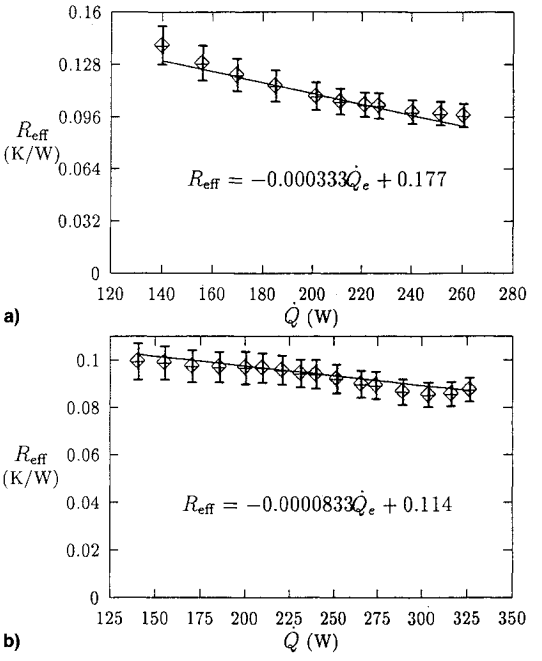

Fig. 6 Effective thermal resistance for T_v = a) 40 and b) 50°C.

For both T_v = 40 and 50°C, the temperature difference increased with the input power. As previously stated, the condenser section temperature remained relatively constant while the evaporator temperature increased with $\dot{Q}_e$. At the lower power levels, ΔT_{cc} was higher for T_v = 40°C. As the power input increased, however, the difference between the two vapor temperatures decreased. This shows that a lower limit of power input exists, below which the LHP will not operate properly. Meyer et al.[7] also reported a similar behavior in which a large step heat input was required in some instances for startup.

The effective thermal resistance was calculated from the experimental results using

$$R_{\text{eff}} = (T_e - T_c)/\dot{Q}_e \tag{11}$$

where T_e and T_c are the average evaporator and condensor temperatures, respectively. For both vapor temperatures (Fig. 5b), the effective thermal resistance decreased with increasing input power. However, near the dryout point for T_v = 50°C, the effective thermal resistance increased slightly. At this point, the liquid menisci began to recede into the capillary wick structure, indicating the onset of dryout. Therefore, this shows that the LHP has an optimal operating condition where the effective thermal resistance is lowest. Meyer et al.[7] reported a similar trend where the effective thermal resistance decreased to a minimum value and then increased.

The uncertainty of the effective thermal resistance was calculated using the rss error. The maximum uncertainty of the effective thermal resistance was found to be 8.5%. Figure 6 shows the effective thermal resistance plotted as a function of the input power and the equation of the least-squares best-fit line for the thermal resistance.

The minimum thermal resistance achieved with the LHP studied in the present experiment was approximately R_{eff} = 0.085 K/W. Dickey and Peterson[6] performed a series of tests on an LHP. The condenser temperature was held constant at 0 and 30°C and adverse tilt angles established a maximum hydraulic head of 0.61 m. The maximum input power of this experiment was $\dot{Q}_e$ = 170 W with the lowest effective thermal resistance of R_{eff} = 0.1 K/W. Maidanik et al.[5] performed tests on two LHPs. In the first of these tests, the coolant temperature was held constant at T_{cf} = 0, 30, and −15°C while the power was increased from $\dot{Q}_e$ = 5 to 300 W. The lowest effective thermal resistance of this LHP was R_{eff} = 0.07 K/W. Meyer et al.[7] tested an LHP with the evaporator directly above the condenser while holding the condenser at T_c = 10 and 30°C. The maximum input power was $\dot{Q}_e$ = 1129 W, with the lowest thermal resistance measuring at R_{eff} = 0.0125 K/W with $\dot{Q}_e$ = 600 W. The maximum stable heat flux reached in the present experiment was $\dot{q}_{e,\max}$ = 12.6 W/cm², which is a significant improvement over that reported by the previous researchers. This may be due to changes in the inverted meniscus wick structure.

The evaporative heat transfer coefficient for an inverted meniscus was calculated from the results of the tests performed on the LHP using

$$h_{\text{eff}} = \frac{\dot{Q}_e}{\pi DL(T_e - T_v)} \tag{12}$$

The heat transfer coefficient for each case was calculated and is shown in Fig. 7. The maximum percent error in the heat transfer coefficient was calculated to be 15.8%. The heat transfer coefficients for both vapor line temperatures remained almost constant as the input power increased. This was illustrated by the very small slope of the best-fit line. For T_v = 40°C, the evaporative heat transfer coefficient ranged from 5221 to 6158 W/m² K, while that at T_v = 50°C varied from 5969 to 6285 W/m² K. The mean values were 5800 and 6200 W/m² K for T_v = 40 and 50°C, respectively.

A finite element model was used to simulate the evaporator section at T_v = 40 and 50°C and was compared to the experimental results obtained from the LHP. The thermal conductivity of the cast aluminum saddle and the stainless steel do not change significantly within the temperature range; therefore, constant values of k_a = 169 W/m K and k_{ss} = 15.6 W/m K were used.[9]

It was assumed that the evaporator was covered with thermal grease and "push-fit" for all but 0.03175 mm of the evaporator length. The remaining 0.03175 mm was force-fit to secure the evaporator inside the aluminum saddle. Oberg et al.[10] gave the tolerances for a push-fit using the difference between the o.d. of the evaporator and the diameter of the hole in the aluminum saddle to be $t_g = 2.54 \times 10^{-6}$ m. An

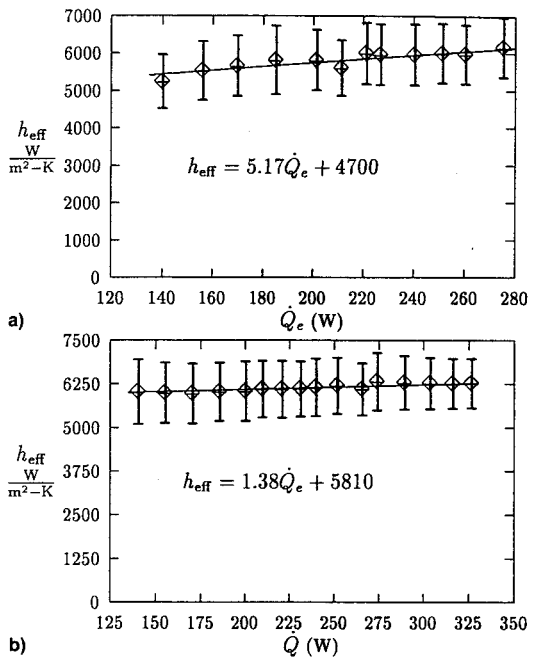

Fig. 7 The experimental evaporative heat transfer coefficient for an inverted meniscus for T_v = a) 40 and b) 50°C.

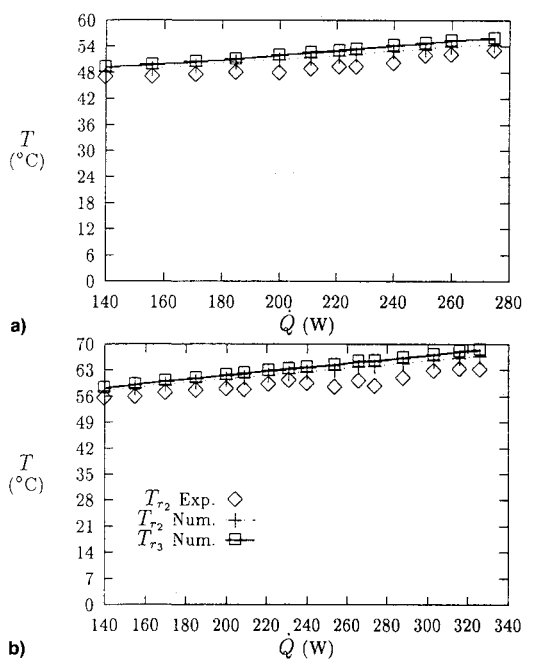

Fig. 8 Comparison of the experimental and numerical results at y = 0 and $r = r_2$ and r_3 for T_v = a) 40 and b) 50°C.

average value for thermal conductivity of the thermal grease was found to be k_g = 0.2678 W/m K.[11] The evaporative heat transfer coefficients presented in Fig. 7 were applied to the numerical model as the evaporative boundary condition using the appropriate vapor line temperature and input power.

Figures 8a and 8b compare the experimental results of the average evaporator temperature at y = 0 and $r = r_2$, and the results of the numerical model at y = 0 and $r = r_2$ and r_3. The first point at y = 0 and $r = r_2$ was located at the outer wall of the evaporator, which was the approximate location of the thermocouples. The second location y = 0 and $r = r_3$ was the interface of the thermal grease and the aluminum saddle. Since the precise location of the thermocouples was not known, both numerical temperatures were plotted to ensure an appropriate comparison between the model and the experimental data. The temperatures given by the numerical model increased linearly as the input power increased. The maximum difference between the experimental results and the numerical results at $r = r_2$ for T_v = 40 and 50°C are 6.5 and 9.4%, respectively. The difference between the temperatures of the experimental data compared to the numerical results at $r = r_2$ were probably caused by the epoxy that held the thermocouples in place. The epoxy (not included in the numerical model) had a lower thermal conductivity than any of the other materials in the evaporator section, so that the temperature gradients near the thermocouples were not as steep as in the aluminum saddle. Figure 9 shows the typical contour plots of the evaporator section for T_v = 40 and 50°C. As expected, the highest temperatures were found directly under the heater. The lowest temperatures were found along the inner wall of the evaporator, which was the location of the convective boundary condition.

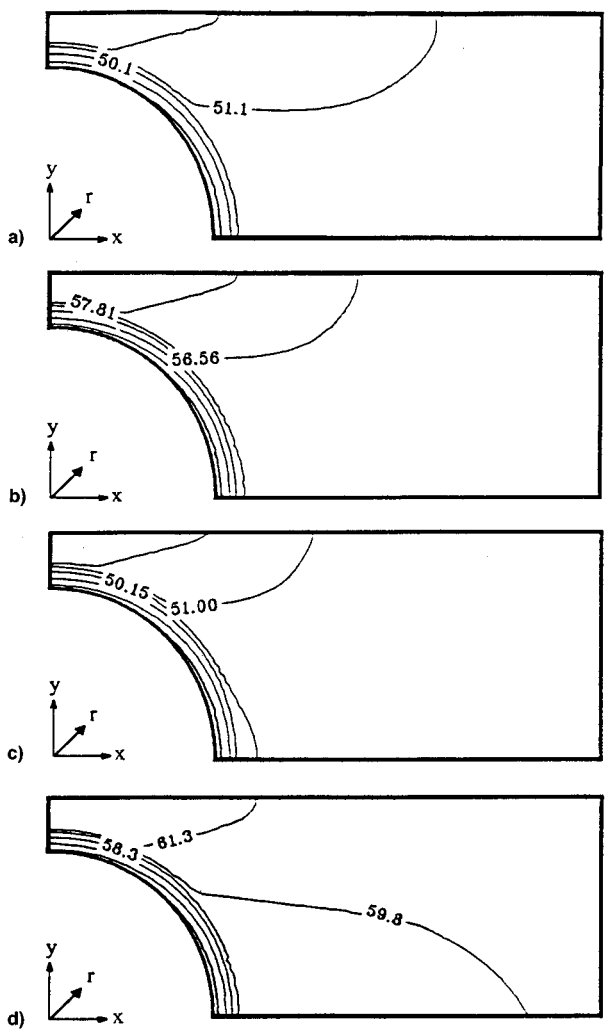

Fig. 9 Typical contour plot of the evaporator section for a) T_v = 40°C and $\dot{Q}_e$ = 171 W, b) T_v = 40°C and $\dot{Q}_e$ = 260 W, c) T_v = 50°C and $\dot{Q}_e$ = 170 W, and d) T_v = 50°C and $\dot{Q}_e$ = 325 W.

Conclusions

The experiments performed on the stainless steel/ammonia LHP demonstrated the operating characteristics. By maintaining a constant vapor temperature, future analytical and numerical models can be compared to the results provided. Dryout was shown to occur at heat inputs near $\dot{Q}_{e,dry}$ = 337 W ($\dot{q}_{e,dry}$ = 13.1 W/cm²) for a vapor temperature of T_v = 50°C. The LHP's best effective thermal resistance was found

to be $R_{\text{eff}} = 0.085$ K/W at $Q_e = 303$ W and $T_v = 50$°C. The data supported the conclusion that the LHP has an optimal operating condition where the effective thermal resistance is minimized.

The numerical model of the evaporator section was validated using the experimental results. The maximum differences between the experimental and numerical results were 6.5 and 9.4% for $T_v = 40$ and 50°C, respectively. The contour plots supported the conclusions that the steepest temperature gradients were found on the evaporator side of the domain (left-hand side), as well as the maximum and minimum temperatures throughout the evaporator section were found at the heater interface and inner wall of the evaporator, respectively.

Acknowledgements

Funding for this work was provided by the Ohio Board of Regents through the Ohio's Research Challenge Grant.

References

[1]Gaugler, R., "Heat Transfer Device," U.S. Patent 2350348, 1944.

[2]Stenger, F. J., "Experimental Feasibility Study of Water-Filled Capillary Pumped Heat Transfer Loops," NASA X-1310, NASA LeRC, 1966.

[3]Maidanik, F., et al., "Heat Transfer Apparatus," U.S. Patent 4515209, 1985.

[4]Ernst, D. M., Phillips, A. L., and Rozin, I. S., "Loop Heat Pipes—Their Potential," DTX Corp. Rept., Lancaster, PA, 1994.

[5]Maidanik, F., Fershtater, G., and Goncharov, K. A., "Capillary-Pump Loop for the Systems of Thermal Regulation of Spacecraft," *Proceedings of the 4th European Symposium on Space Environmental and Control Systems*, European Space Agency, ESA Paper SP-324, 1991.

[6]Dickey, J. T., and Peterson, G. P., "An Experimental and Analytical Investigation of the Operational Characteristics of a Capillary Pumped Loop," AIAA Paper 93-2746, 1993.

[7]Meyer, R., Muller, R., and Beckmann, K., "Investigation of the Heat Transfer Performance of a Capillary Pumped Ammonia Loop Under Gravity," *Proceedings of the 23rd International Conference of Environmental Systems*, Society of Automotive Engineers, 1993 (SAE Paper 932304).

[8]Wirsch, P. J., "An Experimental and Numerical Investigation of a Stainless Steel/Ammonia Loop Heat Pipe," M.S. Thesis, Wright State Univ., Dayton, OH, 1995.

[9]Incropera, F. P., and De Witt, D. P., *Fundamentals of Heat and Mass Transfer*, 3rd ed., Wiley, New York, 1990.

[10]Oberg, E., Jones, F. D., and Horton, J. L., *Machinery's Handbook*, 21st ed., Industrial Press, Inc., New York, 1982.

[11]Veilleux, E. D., "Use of Thermal Greases to Conduct Heat Across Sheet-Metal Interfaces," *Journal of Spacecraft and Rockets*, Vol. 5, No. 10, 1968, pp. 1238–1240.